PHYSICAL REVIEW C VOLUME 52, NUMBER 1 JULY 1995

Charge-changing fragmentation of 10.6 GeV/nucleon ^{197}Au nuclei

L.Y. Geer,[1,*] J. Klarmann,[1] B.S. Nilsen,[2,†] C.J. Waddington,[2] W. R. Binns,[1] J.R. Cummings,[3] and T.L. Garrard[3]

"UHIC Collaboration"

[1] *Department of Physics and McDonnell Center for the Space Sciences, Washington University, St. Louis, Missouri 63130*
[2] *School of Physics and Astronomy, University of Minnesota, Minneapolis, Minnesota 55455*
[3] *George E. Downs Laboratory, California Institute of Technology, Pasadena, California 91125*
(Received 27 December 1994)

We have measured the charge-changing cross sections of 10.6 GeV/nucleon ^{197}Au nuclei interacting in targets of CH_2 (polyethylene), C, Al, Cu, Sn, and Pb. Cross sections for H are calculated from those measured in C and CH_2. The total charge-changing cross sections are higher than those measured at energies of ≤ 1 GeV/nucleon. The measured cross sections for the heavier targets are somewhat larger than those predicted by a model based on data taken at lower energies with lighter targets. Partial charge-changing cross sections for the production of fragments from the incident Au projectiles were measured for charge changes (ΔZ) from $\Delta Z = +1$, $_{80}$Hg, down to approximately $\Delta Z = -29$, $_{50}$Sn. In comparison to lower energy measurements, these partial cross sections are found to be smaller for small ΔZ and larger or the same for large ΔZ. The H partial cross sections are found to follow a power law in ΔZ similar to that for heavier targets, instead of the exponential form observed at lower energies. Factorization is found to hold for all partial cross sections with ΔZ greater than two. In the heavier targets, the cross sections for one and two proton removal have significant contributions from electromagnetic dissociation. The electromagnetic dissociation contribution to the total cross section is derived and found to be relatively small, but with a strong dependence on the charge of the target nuclei of the form $Z_T^{1.75\pm0.01}$.

PACS number(s): 25.75.+r

I. INTRODUCTION

Until recently, the study at accelerators of the fragmentation of nuclei with $Z > 60$ was limited to energies below ~ 1 GeV/nucleon, the maximum energy available for these nuclei from the Lawrence Berkeley Laboratory Bevalac. Previous experiments [1–4] found that many of the important charge-changing fragmentation cross sections were still varying at this maximum energy, with some exceptions. Clearly, energy independence, also known as limiting fragmentation, for the heavy nuclei could only be reached at energies beyond the range available from the Bevalac. These conclusions were pertinent to several astrophysical problems involving ultraheavy (UH) cosmic ray nuclei ($Z > 30$), since the energy of the average observable UH nucleus greatly exceeds 1 GeV/nucleon. Models of the galactic propagation of cosmic-ray nuclei and of the interactions of these nuclei in detectors and any overlying atmosphere are affected by energy variations in the nuclear cross sections. Although the cross sections measured at the low energies typical of the Bevalac appeared to follow simple trends, there is no comprehensive theoretical understanding of these trends that would allow extrapolation of the measurements to higher energies.

Once the Brookhaven National Laboratory Alternating Gradient Synchrotron (AGS) accelerated ^{197}Au nuclei to an energy of 10.6 GeV/nucleon, it was possible to study the fragmentation of nuclei at an energy more typical of those observed in the cosmic rays. With an array of detectors similar to that used at the Bevalac, we were able to study the interactions of these Au nuclei in a wide range of targets. This array was capable of measuring the total cross sections for charge change in each target and the partial charge-changing cross sections for the fragmentation of Au nuclei to elements with charges from ~ 50 to 80. Preliminary results reported earlier in [5] have been updated and refined here.

These cross sections have been compared directly to lower energy cross sections measured at the Bevalac, as well as to cross sections measured in etchable glass detectors by Hirzebruch *et al.* [6] and He and Price [7] using similar, approximately 10 GeV/nucleon ^{197}Au beams. The partial cross sections in hydrogen have also been compared to those predicted by the semiempirical calculations of Silberberg and Tsao [8], often used in models of cosmic-ray propagation.

In addition to these comparisons, the electromagnetic contribution to the total cross section was estimated. At this energy, a considerable electromagnetic pulse is gener-

*Present address: Department of Molecular and Cell Biology, Division of Neurobiology, University of California at Berkeley, Berkeley, CA 94720.
†Present address: Department of Physics and Astronomy, Louisiana State University, Baton Rouge, LA 70803.

ated by heavy target nuclei. However, the high Coulomb barrier of Au should impede any electromagnetic dissociation (EMD) that results in charge change. The contribution of such charge-changing EMD to the total cross sections was calculated by assuming the nuclear components of the partial cross sections can be factored into terms depending only on target or fragment, known as factorization. This assumption allowed an estimation of the nuclear contribution to the partial cross sections by extrapolating partial cross sections with minimal EMD to those with substantial EMD. Although factorization was not found applicable in our previous studies [2,4], it has been found in other studies of nuclear fragmentation [9], particularly in the relativistic collisions of light nuclei. The target dependence of the EMD cross sections could then be compared to calculations using the Weizsäcker-Williams virtual photon method [10]. Also, after subtraction of the EMD contributions, the nuclear part of the total charge-changing cross sections could be better fit with semiempirical expressions, such as hard-sphere models [11].

II. EXPERIMENT

The layout of the detectors for AGS experiment 869 is shown in Fig. 1. The length of the entire array was $\sim$ 2.75 m. Three types of detectors were used in this array: parallel plate ion chambers filled with P-10 counting gas, light diffusion box Cherenkov detectors using Pilot 425 radiators, and multiwire proportional chambers (MWPC's) filled with 80/20 Ar/CO_2. These detectors were essentially identical in construction to those used by us in previous experiments [1,3,4]; further details can be found in Geer [12]. In thickness, the Cherenkov

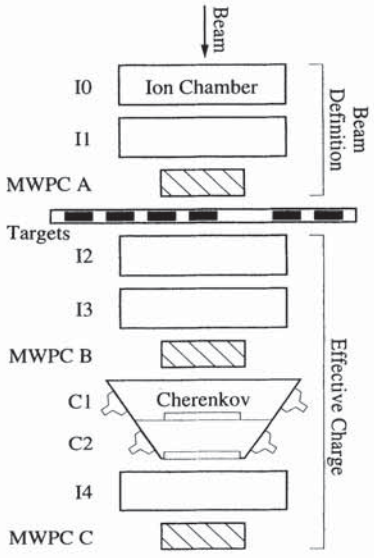

FIG. 1. Layout of the experiment. $I0$, $I1$, $I2$, $I3$, and $I4$ are parallel plate ion chambers. MWPC's A, B, and C are multiwire proportional chambers. $C1$ and $C2$ are Cherenkov counters.

detectors were $\sim$ 0.15 interaction lengths of Au(λ_{Au}), the ion chambers $\sim 3 \times 10^{-3}\lambda_{AU}$, and the MWPC's $\sim 1 \times 10^{-3}\lambda_{Au}$, each. The detector signals were acquired by a multichannel analog converter and recorder. Initially, data acquisition was triggered when a signal in any detector was above the noise; later, to reduce the data rate, the acquisition was triggered only when the signal from the first ion chamber ($I0$) was above the noise.

The array can be considered in three sections: beam definition, target, and effective charge measurement. The beam definition section was used to select a beam of Au nuclei with a limited spatial distribution. The charges of the incident projectiles were measured in the first two ion chambers, and any contamination was removed in the data analysis. The transverse spatial distribution of the beam was determined by the first MWPC, allowing the removal of any particles that fell outside the defined area of the beam.

The target section consisted of a remotely controlled mechanical target changer which held targets of CH_2 (polyethylene), C, Al, Cu, Sn, and Pb. One target holder was left vacant for a targetless exposure ("blank run") used to correct for interactions in the detector array. Characteristics of the targets are detailed in Table I; each was chosen to be $\sim 0.20\lambda_{Au}$, as a compromise between maximizing the number of interactions and minimizing the corrections needed for secondary interactions in the target. Hydrogen cross sections were obtained by subtraction of the cross sections found in C from those in CH_2 using

$$\sigma(\mathrm{H}) = \tfrac{1}{2}[3\sigma(\mathrm{CH_2}) - \sigma(\mathrm{C})]. \quad (1)$$

The final section of the array was composed of the effective charge measurement detectors, in which the effective charge

$$Z' = \left(\sum_{i=1}^{n} Z_i^2\right)^{1/2} \quad (2)$$

was determined for the n forwardly projected projectile fragments and produced particles of charge Z_i exiting the target through the array. The effective charge was measured by summing combinations of weighted signals from the two rear ion chambers, $I3$ and $I4$, and the two Cherenkov counters, $C1$ and $C2$. Since the signals for both types of detectors were proportional to the squares

TABLE I. The thicknesses of the targets, the total cross sections of 10.6 GeV/nucleon Au, and fitted target factors with reduced χ^2.

Target	Thickness (g/cm^2)	$\sigma(T)$ (mb)	γ_T	χ^2/ν
H		1572 ± 31	1	
CH_2	0.777 ± 0.007	2003 ± 21		
C	1.522 ± 0.004	2866 ± 19	1.069 ± 0.015	0.9
Al	2.483 ± 0.005	3601 ± 23	1.174 ± 0.014	1.1
Cu	4.685 ± 0.008	4576 ± 28	1.333 ± 0.016	1.7
Sn	7.52 ± 0.01	5572 ± 35	1.477 ± 0.018	1.3
Pb	10.61 ± 0.01	6935 ± 36	1.639 ± 0.019	1.1

of the charges, it can be assumed that the sum in Eq. (2) is dominated by the most highly charged fragment for charge change $|\Delta Z| < 30$. This assumption is justified by the excellent charge resolution observed experimentally for such interactions and from calculations of the effective charge distribution using data from nuclear emulsion studies of the same projectiles where all the particles emitted can be observed individually [13]. The signals from the two rear ion chambers were used to identify those fragments that interacted in the Cherenkov counters.

It should be noted that electronic charge capture (ECC) of the projectile was not an important effect in this experiment as the calculated mean free path in carbon for electron stripping is ~ 0.4 mm while the mean free path for electron capture is ~ 100 mm [6]. Because of this difference, the significant amount of matter in the effective charge section ($> 0.3\lambda_{\mathrm{Au}}$) rapidly stripped any attached electron and resulted in a measured charge extremely close to the actual charge.

The data were collected in two series of target exposures, the second done at a much higher event rate and containing at least double the number of events. Both series showed excellent charge resolution in the Cherenkov counters, better than 0.18 charge units. Good charge resolution was especially important in separating the small $\Delta Z = +1$ peak from the dominant beam peak in the histogram of effective charge. In the first series of exposures the separation was clear, with the minima reaching zero counts after background subtraction. The second series showed slightly worse resolution; therefore the signals from $I3$ and $I4$, statistically weighted by their individual resolutions, were included in the sum of signals to further improve the charge resolution. This addition yielded a charge resolution of better than 0.15 charge units with clear minima between the beam peak and the $\Delta Z = +1$ peak. An effective charge histogram for a CH_2 exposure in the second series is shown in Fig. 2 before background subtraction and illustrates the clear separation between neighboring charges.

Two systematic deviations of the signal levels for the charge peaks were noticed in the detectors. The first deviation varied with target and affected the mean and standard deviation of the average pulse height for all fragments. Since the deviation was greatest in detectors closest to and downstream from the target, it was hypothesized to be the result of knock-on electron production in the target. The effect on the standard deviation of the average signal was minor and did not significantly affect charge resolution, but the mean signal for some target exposures increased over the targetless exposures by as much as 10% in $I2$ to as little as 1% in the Cherenkov detectors. A satisfactory correction to this variation was accomplished by normalizing the signals for a given detector using the average signal of noninteracting Au nuclei that passed through the detector.

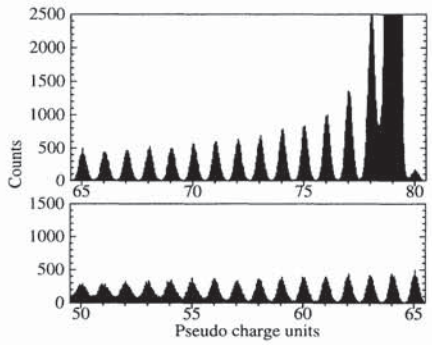

FIG. 2. Histogram of effective charge for a CH_2 exposure to 10.6 GeV/nucleon Au showing charge resolution for the ion chambers and Cherenkov detectors in the effective charge section.

The second deviation was a beam rate dependence of the signal from the Cherenkov counters, with a higher signal for higher beam intensities. The variation was a fraction of a charge unit. To satisfactorily correct for this effect, the Cherenkov signals for all events in each beam pulse were normalized using the average Au signal for that beam pulse. The beam pulses were approximately 1 sec in duration and typically contained a few thousand Au nuclei.

III. ANALYSIS

A. Beam selection

The first step in the analysis was the selection of the projectile beam nuclei. The incident beam of Au nuclei was defined by requiring the sum of the signals from the first two ionization chambers, $I0$ and $I1$, to be within 1.5 standard deviations (s.d.) of the peak values, found by fitting a Gaussian to the distribution of signals produced by the incident projectiles. The s.d. was approximately 0.2 charge units. This selection removed 13% of the Au nuclei along with all of the events triggered by non-Au particles, which comprised $\sim 7\%$ of the total number of events. The location of the beam was defined to be within 2 s.d. of the centroid in both the x and y directions of MWPC A, where the spatial distribution was Gaussian with s.d. ~ 0.75 c.m. The small beam size allowed us to measure all fragments of interest and to ignore positional effects in the detector, since emulsion experiments show that essentially none of the fragments with $Z > 40$ are emitted more than 8 mrad from the beam direction [13]. Hence, even in $I4$, the detector most downstream, none of the fragments diverged more than 1.3 cm, and any spatial gradients in response in any of the detectors could be neglected.

B. Total cross sections

The total charge-changing cross sections were measured by counting the number of noninteracting particles in the target exposure and using a targetless exposure to determine the number of particles that interacted in material other than the target. For a target exposure, the number of gold nuclei counted in the Cherenkov detectors is given by

$$N = N_0 k_1 k_2 \exp(-x_M/\lambda_M) \exp(-x_T/\lambda_T), \quad (3)$$

where N_0 is the number of incident projectile particles, x_M is the thickness and λ_M is the mean free path of Au nuclei in the material between the target and Cherenkov radiator $C1$, and x_T and λ_T are the thickness and mean free path of the target T. The constant k_1 accounts for particles that interacted in the Cherenkov detectors but were counted as gold nuclei because their effective charge was sufficiently close to that of Au. The correction factor k_2 represents gold nuclei in the tails of the gold peak not included in the selection on the Cherenkov counter signals. A similar expression to Eq. (3) exists for the targetless exposure:

$$N' = N'_0 k_1 k_2 \exp(-x_M/\lambda_M), \quad (4)$$

where N' is the number of Au nuclei in the Cherenkov counters and N'_0 is the number of incident projectile particles. Dividing (3) by (4) eliminates several terms and we obtain

$$\lambda_T = x_T \left(\ln \frac{N_0 N'}{N'_0 N} \right)^{-1}, \quad (5)$$

which is then used to calculate the total cross section $\sigma(T)$ from

$$\sigma(T) = \frac{\langle A_T \rangle}{N_A \lambda_T}, \quad (6)$$

where N_A is Avogadro's number and $\langle A_T \rangle$ is the average atomic mass of the target, assuming natural abundances.

To effectively determine the total cross sections by Eqs. (5) and (6) is it necessary to perform identical selections for Au in both target and targetless exposures. For each exposure, the Cherenkov counter signals were summed and histogrammed, and a Gaussian was fit to the beam peak. The mean and standard deviation of this fit was used to define a ± 3.5 s.d. selection on the Au peak in the Cherenkov counter signals. This selection was then applied to determine either N for the target exposures or N' for the targetless exposures. The results were insensitive to the exact selection used, since a 3.5 s.d. selection extends well into the tails of the beam peak and includes virtually all of the noninteracting beam particles and almost none of the interacting particles.

C. Partial cross sections

Partial cross sections were determined using the same beam definition selections as for the analysis of the total cross sections. The number of fragments of each charge was determined by summing the number of nuclei between the minima of the charge peaks in the effective charge histograms. Although the charge resolution for largest ΔZ was not adequate to completely separate the charge peaks, counting the number of nuclei between minima was an excellent estimation of the true number in each charge peak, as the overlap is so small. Also, since the number of nuclei in each peak varies slowly with effective charge, the small amount of overlap present in a given peak is closely offset by the overlap of the peak itself into adjacent peaks.

Because of the interactions in the material of the detector array, several corrections had to be applied to the measured numbers of fragments produced in order to deduce the partial cross sections. All of these corrections had roughly the same magnitude in all targets, as the targets had similar thicknesses in interaction lengths. These corrections were applied to all the partial cross sections, including those for charge pickup, $\Delta Z = +1$, which have been revised from those discussed in an earlier paper [14].

1. Consistency correction

Because of their excellent charge resolution of less than 0.18 charge units, the Cherenkov counters were the primary detectors used to measure the charges of the fragments. Since these counters had an appreciable thickness of $\sim 0.3\ \lambda_{\mathrm{Au}}$, it was necessary to identify those nuclei that interacted in them by applying a consistency criterion to remove the erroneous effective charges that would have resulted from these interactions. A consistency requirement between the signals from ion chambers $I3$ and $I4$, which were mounted on either side of the Cherenkov counters, provided this criterion. Because the consistency selection varied with charge, it was applied by partitioning the sum of signals from $I3$ and $I4$ into several charge ranges. For each of these charge ranges a histogram was generated of the difference in signal between $I3$ and $I4$. These histograms consisted of a central Gaussian resulting from nuclei whose charges remained consistent between $I3$ and $I4$ and a long tail due to nuclei that interacted. The means and standard deviations derived from fitting the Gaussians were used to define a ± 2 s.d. consistency selection for each charge region.

After applying this selection it was necessary to add back the number of particles eliminated to find the true number emitted from the target. This selection was done by fitting the hard-sphere expression of Eq. (10) to the total cross-section data described in this paper and using it to determine the expected number of interactions for each fragment charge. This fit was assumed to have a 10% uncertainty. Typical corrections are shown in Table II for a Pb exposure. The magnitudes of the corrections ranged from ~ 20 to $\sim 30\,\%$ for all targets. The total uncertainties introduced by this correction in the number of fragments for each charge change ranged from 2 to 3 %, depending on the charge of the fragment.

2. Targetless exposure subtraction

A second correction to the data was necessary to compensate for those nuclei that interacted in the nontarget matter between the Cherenkov detectors and the beam definition section of the array. This correction was accomplished by subtracting the histogram of the sum of the signals from $C1$ and $C2$ of the targetless exposure

from the target exposure, normalizing the counts in the targetless exposure to have the same number of Au nuclei in the Cherenkov detectors as the target exposure. Typical values for this correction for a Pb target exposure are shown in Table II, and were $\sim 10\%$ for all targets. The cross sections for $\Delta Z = +1, -1$ have larger corrections of $\sim 25\%$ because of a small number of nuclei created in the Cherenkov detectors with $\Delta Z = +1, -1$ that pass the consistency criterion. This effect is only important at the beam peak because of the large number of beam particles. The uncertainties of the correction were the statistical uncertainties of the targetless exposures.

3. *Thick target*

Since the targets typically had an interaction length of 0.20 λ_{Au}, some of the nuclei experienced multiple interactions in the target. To account for these interactions, a program was written to simulate the propagation of the projectile nuclei through a thick target using an initial estimate of the cross sections. The fragment abundances calculated to be exiting the target were compared with the measured fragment abundances and the estimated partial cross sections adjusted to minimize the differences. The process was iterated until the differences were minimal.

To do this, the program treated the target as being divided into 1000 equally thin slabs, each much less than an interaction length. Making the approximation that $x \ll \lambda_T$, where x is the thickness of one slab, then for each slab the change in the number of nuclei entering the slab is

$$\Delta N_F = \sum_{P \geq F} \frac{N_A x}{\langle A_T \rangle} M_{F,P} N_P, \tag{7}$$

where ΔN_F is the change in N_F, the number of nuclei entering the slab, indexed by fragment charge. $M_{F,P}$ is the matrix of cross sections

$$M_{F,P} = \begin{cases} \sigma_{\Delta Z}(T,F,P), & F \neq P \\ -\sigma(T,P), & F = P, \end{cases} \tag{8}$$

where $\sigma(T,P)$ is the total charge-changing cross section for projectile P in target T and $\sigma_{\Delta Z}(T,F,P)$ is the partial cross section for projectile P changing into fragment F in target T. $\sigma(T,P)$ was calculated using the same expression for the total cross sections used in the consistency selection described in Sec. III C 1. $\sigma_{\Delta Z}(T,F,P)$ was initially approximated by

$$\sigma_{\Delta Z}(T,F,P) = \sigma_{\Delta Z}(T,F,P = \mathrm{Au}) \frac{\sigma(T,P)}{\sigma(T,P = \mathrm{Au})}, \tag{9}$$

where the partial cross sections for Au were calculated from the measured abundances assuming an infinitely thin target. Using this initial $M_{F,P}$ and Eq. (7), projectile particles were propagated through all 1000 slabs and abundances calculated for nuclei exiting the target. These calculated abundances were compared to the actual abundances and $M_{F,P}$ adjusted to attempt to compensate for the differences. The procedure was iterated until the calculated and measured abundances converged, with the result that $M_{F,P}$ yielded our final cross sections. The corrections ranged from $\sim 25\%$ of the number of particles for small ΔZ to $\sim 10\%$ for large ΔZ. Typical values are listed in Table II for a Pb exposure. The uncertainties for this thick target correction were 10% of the corrections themselves; thus the uncertainties introduced by this correction in the number of fragments for each charge ranged from ~ 2.5 to $\sim 1\,\%$.

TABLE II. Corrections for a typical Pb target exposure. Shown for each correction is the percent change in the number of fragments with charge change ΔZ.

ΔZ	Targetless exposure subtraction (% correction)	Consistency (% correction)	Thick target (% correction)
1	−28	33	23
−1	−21	33	23
−2	−9	32	20
−3	−11	32	20
−4	−11	32	20
−5	−10	31	20
−6	−7	31	20
−7	−11	31	19
−8	−10	30	19
−9	−12	30	19
−10	−12	29	18
−11	−8	29	19
−12	−7	29	19
−13	−7	29	19
−14	−11	28	17
−15	−9	28	18
−16	−10	27	18
−17	−9	27	16
−18	−11	27	18
−19	−9	26	18
−20	−10	26	17
−21	−8	26	18
−22	−11	26	16
−23	−9	25	17
−24	−7	25	17
−25	−9	24	17
−26	−8	24	16

IV. RESULTS

A. Total cross sections

The total charge-changing cross sections and their uncertainties are listed in Table I. The uncertainties combine both the statistical uncertainties and the systematic uncertainties from the measurements of the target thicknesses and densities. The statistical uncertainties were frequently dominant. In Fig. 3, the cross sections are compared to values measured by Binns *et al.* [3] at ~ 1 GeV/nucleon, and the predictions from two semiempirical expressions. The cross sections measured in this

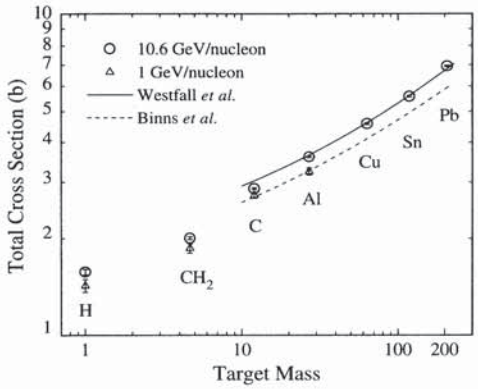

FIG. 3. Measured data and semiempirical expressions for Au total charge-changing cross sections on various targets. Binns *et al.* [3] data were taken at approximately 1 GeV/nucleon. The Westfall *et al.* [15] expression was obtained form 1.88 GeV/nucleon Fe data. The Binns *et al.* expression was obtained using several heavy projectiles at maximum Bevalac energies.

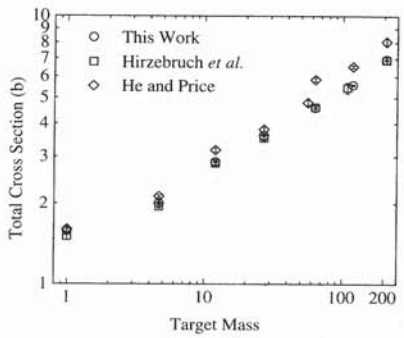

FIG. 4. Comparison of the 10.6 GeV/nucleon total cross sections to the measured total cross sections of Hirzebruch *et al.* [6] and He and Price [7] as a function of the mass of the target.

experiment are significantly higher than those measured at $\sim$ 1 GeV/nucleon. The greatest difference is for the Al target, the heaviest used at the lower energy. For the heavier targets, the cross sections also appear to deviate from the expressions that represented the best fits to the low-energy values.

The semiempirical expression of Westfall *et al.* [15] is a hard-sphere model with the form

$$\sigma(T) = \pi {r_0}^2 (A_T^{1/3} + A_P^{1/3} - b)^2, \tag{10}$$

where A_T is the atomic mass of the target and A_P is the atomic mass of the projectile. r_0 and B are parameters with values $r_0 = 1.35 \pm 0.02$ fm and $b = 0.83 \pm 0.12$. The Binns *et al.* [3] semiempirical expression is similar to Eq. (10) but has a mass-dependent overlap term

$$\sigma(T) = \pi {r_0}^2 \left(A_T^{1/3} + A_P^{1/3} - d(A_T + A_P)^{1/3} \right)^2 \tag{11}$$

with r_0 fixed at 1.35 fm and $d = 0.209 \pm 0.002$. The Westfall *et al.* expression was fit to the total charge-changing cross sections of 1.88 GeV/nucleon ^{56}Fe incident on a wide range of targets and the Binns *et al.* expression was fit to the charge-changing cross sections of Kr, Xe, Ho, and Au projectiles at Bevalac energies on targets of Al and lighter. Neither expression consistently fits the cross sections measured in this study within the uncertainties. However in Sec. IV C both expressions will be refit to the cross sections after the electromagnetic dissociation contribution has been subtracted.

The total cross sections can also be compared to those measured by Hirzebruch *et al.* [6] and He and Price [7] using BP-1 glass track detectors with similar Au projectiles from the AGS. This comparison is shown in Fig. 4. The cross sections reported by Hirzebruch *et al.* are in excellent agreement with those reported here, even though our results are measured with a totally different detection system, whereas those of He and Price show serious disagreements with both of these independent determinations. Since the detection techniques used by Hirzebruch *et al.* are essentially identical to those used by He and Price, we have to conclude that the He and Price results must have been affected by some unknown systematic uncertainty. As a consequence we have disregarded the He and Price data in the following discussion.

B. Partial cross sections

The partial cross sections are listed in Table III and shown as a function of ΔZ in Fig. 5. The uncertainties listed include those introduced by the corrections described in Sec. III C. The partial cross sections for charge pickup have been discussed in a previous paper [14]. The partial cross sections $\sigma_{\Delta Z}(T, F)$ for ΔZ from -3 to -20 can be fit with power-law relations of the form

$$\sigma_{\Delta Z}(T, F) = A \cdot |\Delta Z|^{-B}, \tag{12}$$

where A and B are constants fitted for each target and are listed in Table III. The values of B are found to be largely independent of the target mass, but are significantly smaller than the values found at lower energies [2], which are all greater than 0.68. These power laws are not fit to the $\Delta Z = -1$ and -2 cross sections, which clearly deviate and are assumed to be influenced by electromagnetic dissociation (see Sec. IV C).

In comparison to the lower energy values, these high-energy partial cross sections are smaller for small charge changes and larger or equal for large charge changes. This effect is true for all targets used at low energies; typical comparisons are shown in Fig. 6 to data taken at 0.92 GeV/nucleon by Cummings *et al.* [1]. Since the total cross sections are somewhat larger at this higher energy, this implies that the partial cross sections for large charge changes must be appreciably greater at the higher energies. Taking the ratios of the low- and high-energy cross sections emphasizes the differences; the ratios for carbon are shown in Fig. 7. Since we can use carbon to approximate the atmospheric matter overlying a balloon-borne

experiment to measure cosmic-ray abundances, the effects of these differences on the abundances deduced at the top of the atmosphere will be considerable.

The most striking differences between the high- and low-energy cross sections are those for hydrogen. Unlike other targets, the H partial cross sections at lower energies show a roughly exponential dependence on charge change. However, at 10.6 GeV/nucleon the H partial cross sections follow a power law similar to those of heavier targets, as illustrated in Fig. 8. The ratios of these cross sections are shown in Fig. 9, illustrating the very large differences that occur in this energy range. Clearly, calculations of cosmic-ray propagation in the interstellar medium using either of these sets of cross sections will be quite different.

Our measured H partial cross sections can be compared with those calculated from a recent version of the semiempirical codes of Silberberg and Tsao [8], which are primarily based on measurements of the partial cross sections for the production of radioactive isotopes created from the proton bombardment of target nuclei. The ratios of the predicted to the measured cross sections are graphed in Fig. 10 and indicate agreement on the dependence with ΔZ, but with the predicted values lying generally above those measured.

Both Hirzebruch *et al.* [6] and He and Price [7] have measured partial cross sections for a limited range of ΔZ using similar beams. There is general agreement between our cross sections and those of Hirzebruch *et al.*, as shown in Fig. 11. The He and Price partial cross sections are clearly different and are not displayed.

C. Electromagnetic dissociation and factorization

Electromagnetic dissociation occurs when the Lorentz-contracted electric field of the target nucleus contributes to the fragmentation of nuclei. Studies of neutron-producing electromagnetic dissociation interactions for UH nuclei have shown that for high enough relativis-

TABLE III. Partial cross sections for 10.6 GeV/nucleon Au in several targets. Listed underneath are the parameters and reduced χ^2 for power-law fits to the partial cross sections using Eq. (12) in the text.

ΔZ	H (mb)	CH_2 (mb)	C (mb)	Al (mb)	Cu (mb)	Sn (mb)	Pb (mb)
$+1$[a]	10.9 ± 0.7	11.3 ± 0.4	12.1 ± 0.7	16.3 ± 1.0	18.9 ± 1.1	20.4 ± 1.4	23.2 ± 1.4
-1	167 ± 6	175 ± 4	192 ± 5	222 ± 5	277 ± 6	362 ± 8	540 ± 11
-2	93 ± 3	96.9 ± 1.9	104 ± 3	120 ± 3	137 ± 3	161 ± 4	195 ± 4
-3	72 ± 2	73.5 ± 1.5	77 ± 2	89 ± 2	102 ± 3	110 ± 3	125 ± 3
-4	56 ± 2	59.7 ± 1.2	66.4 ± 1.8	69 ± 2	76 ± 2	91 ± 3	101 ± 3
-5	51.6 ± 1.8	52.5 ± 1.1	54.4 ± 1.6	56.9 ± 1.7	69 ± 2	72 ± 2	80 ± 2
-6	43.7 ± 1.6	46.2 ± 0.9	51.3 ± 1.5	55.9 ± 1.7	67 ± 2	71 ± 2	77 ± 2
-7	41.0 ± 1.5	42.4 ± 0.9	45.1 ± 1.4	49.8 ± 1.6	55.9 ± 1.8	62 ± 2	68 ± 2
-8	40.1 ± 1.4	40.0 ± 0.8	39.8 ± 1.3	44.0 ± 1.5	47.2 ± 1.6	55 ± 2	62 ± 2
-9	35.1 ± 1.3	36.2 ± 0.7	38.3 ± 1.2	41.9 ± 1.4	49.4 ± 1.6	52 ± 2	57.0 ± 1.9
-10	33.6 ± 1.2	33.9 ± 0.7	34.6 ± 1.2	37.5 ± 1.3	46.4 ± 1.6	50.1 ± 1.9	55.0 ± 1.8
-11	32.9 ± 1.2	32.8 ± 0.7	32.8 ± 1.1	39.6 ± 1.3	39.2 ± 1.4	46.1 ± 1.8	50.6 ± 1.7
-12	31.6 ± 1.1	31.3 ± 0.6	30.7 ± 1.1	33.7 ± 1.2	39.9 ± 1.4	42.9 ± 1.7	48.7 ± 1.7
-13	28.8 ± 1.1	29.4 ± 0.6	30.6 ± 1.1	32.7 ± 1.2	37.2 ± 1.4	42.0 ± 1.7	49.1 ± 1.7
-14	27.9 ± 1.0	28.9 ± 0.6	30.9 ± 1.1	33.9 ± 1.2	39.7 ± 1.4	43.8 ± 1.7	45.9 ± 1.6
-15	27.7 ± 1.0	28.7 ± 0.6	30.8 ± 1.1	33.5 ± 1.2	35.8 ± 1.3	40.2 ± 1.6	44.8 ± 1.5
-16	25.2 ± 1.0	25.9 ± 0.5	27.2 ± 1.0	31.7 ± 1.2	34.0 ± 1.3	36.9 ± 1.6	42.1 ± 1.5
-17	24.9 ± 0.9	25.7 ± 0.5	27.5 ± 1.0	28.9 ± 1.1	34.2 ± 1.3	41.1 ± 1.7	38.7 ± 1.5
-18	24.2 ± 0.9	25.0 ± 0.5	26.7 ± 1.0	29.3 ± 1.1	32.7 ± 1.3	34.7 ± 1.6	41.0 ± 1.5
-19	23.4 ± 0.9	24.2 ± 0.5	25.8 ± 1.0	26.9 ± 1.1	31.8 ± 1.2	33.6 ± 1.5	40.8 ± 1.5
-20	23.8 ± 0.9	23.8 ± 0.5	23.7 ± 0.9	26.9 ± 1.1	30.0 ± 1.2	33.9 ± 1.5	37.6 ± 1.4
-21	22.9 ± 0.9	23.3 ± 0.5	24.1 ± 0.9	27.6 ± 1.1	26.7 ± 1.1	34.7 ± 1.5	39.3 ± 1.4
-22	21.6 ± 0.8	21.9 ± 0.5	22.5 ± 0.9	26.2 ± 1.0	22.9 ± 1.0	31.2 ± 1.4	38.8 ± 1.5
-23	23.5 ± 0.9	24.7 ± 0.5	26.9 ± 1.0	26.9 ± 1.0	32.8 ± 1.2	35.5 ± 1.5	40.0 ± 1.4
-24	23.7 ± 0.9	24.2 ± 0.5	25.4 ± 0.9	32.8 ± 1.1	35.4 ± 1.3	35.7 ± 1.5	45.3 ± 1.5
-25	23.8 ± 0.9	24.2 ± 0.5	25.1 ± 0.9	29.3 ± 1.1	30.9 ± 1.2	40.9 ± 1.7	38.4 ± 1.4
-26	21.3 ± 0.8	22.6 ± 0.5	25.3 ± 0.9	28.1 ± 1.1		32.1 ± 1.4	41.2 ± 1.5
-27	23.3 ± 0.8	23.7 ± 0.5	24.6 ± 0.9			37.3 ± 1.5	
-28	20.2 ± 0.8	21.1 ± 0.4	22.9 ± 0.9				
-29	19.1 ± 0.8	20.1 ± 0.4	22.0 ± 0.9				
-30		20.3 ± 0.4					
A	129 ± 5	135 ± 3	148 ± 5	161 ± 6	188 ± 7	208 ± 8	230 ± 7
B	0.58 ± 0.02	0.59 ± 0.01	0.61 ± 0.02	0.60 ± 0.02	0.62 ± 0.02	0.62 ± 0.02	0.61 ± 0.01
χ^2/ν	0.7	1.1	1.6	2.0	2.5	1.5	1.8

[a]These cross sections have been revised from those reported in [14].

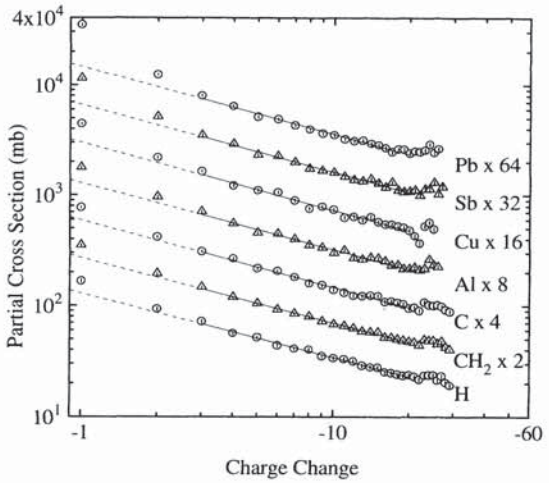

FIG. 5. Partial cross sections for 10.6 GeV/nucleon Au on different targets as a function of charge change. For display, the cross sections for a given target are multiplied by the number next to the target symbol. Power laws are fit to cross sections from $\Delta Z = -3$ to -20 as these cross sections are likely to be unaffected by electromagnetic dissociation.

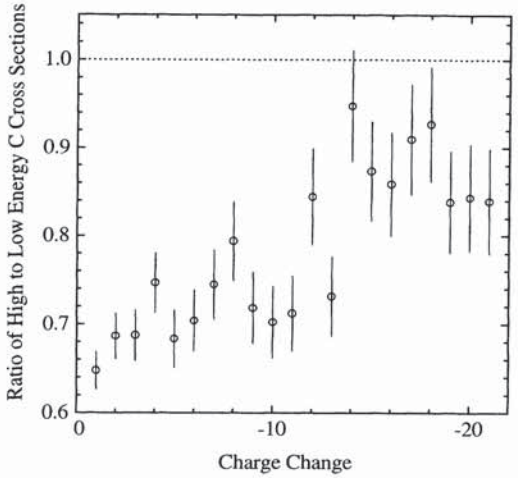

FIG. 7. Ratios of the partial cross sections for Au in a C target at 10.6 GeV/nucleon to those measured at 0.92 GeV/nucleon [1] vs charge change.

tic energies the electromagnetic contribution to the total interaction cross section can exceed the nuclear contribution [16]. However, *charge-changing* electromagnetic dissociation (EMD) has not been studied thoroughly for UH nuclei, where the high Coloumb barrier should be an impediment [17,18]. The EMD contribution to the present cross sections can be estimated by assuming that the EMD contribution to the H cross sections is negligible and that the nuclear portion of the cross sections can be factored. Calculations using the Weizsäcker-Williams virtual photon method [10] are difficult in this case due to the lack of proton photodissociation cross sections for Au. Calculations of the photodissociation cross sections using statistical decay code will have large uncertainties.

Previous studies [9,19,20], including those using Au targets bombarded with relativistic ions [21], have demonstrated that in some cases the nuclear portion of the partial cross sections $\sigma_{\Delta Z}(T,F)$ for a given projectile can be separated into factors γ^F, depending only on the fragment, and γ_T, depending only on the target, so that

$$\sigma_{\Delta Z}(T,F) = \gamma^F \gamma_T + \sigma_{\mathrm{EMD}}(T,F), \tag{13}$$

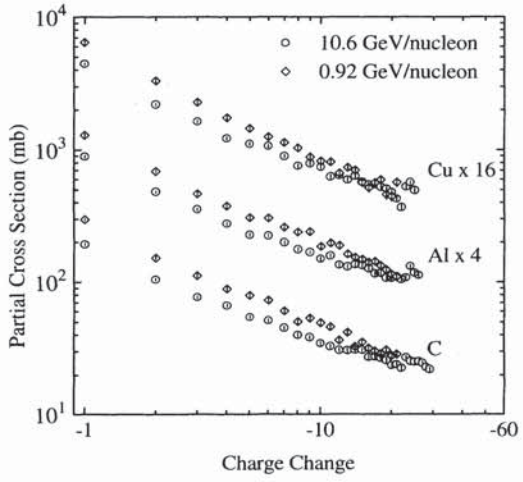

FIG. 6. Comparison of 10.6 GeV/nucleon Au partial cross sections to data taken at 0.92 GeV/nucleon [1] as a function of charge change. For display purposes, the cross sections for a given target are multiplied by the number next to the target symbol.

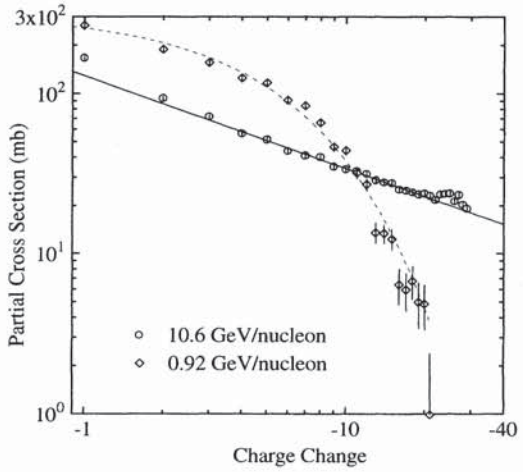

FIG. 8. Comparison of H partial cross sections for 10.6 GeV/nucleon Au to data taken at 0.92 GeV/nucleon [1] as a function of charge change. To guide the eye, the 10.6 GeV/nucleon data are fit with a power law (solid line) and the 0.92 GeV/nucleon data are fit with an exponential (dashed line).

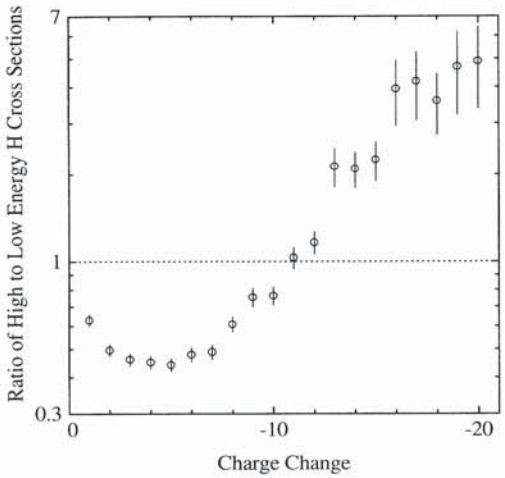

FIG. 9. Ratios of the partial cross sections for 10.6 GeV/nucleon Au in a H target to those measured at 0.92 GeV/nucleon [1] vs charge change.

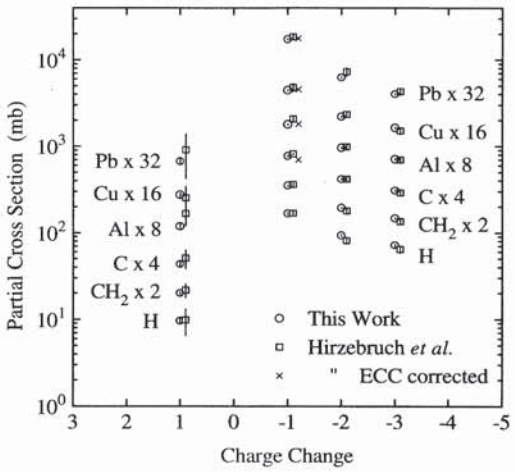

FIG. 11. Comparison of the partial cross sections for 10.6 GeV/nucleon Au to those measured by Hirzebruch *et al.* [6] as a function of charge change. For display purposes, the cross sections for a given target are multiplied by the number next to the target symbol and displaced from their integer values. Also displayed are the Hirzebruch *et al.* cross sections corrected for electronic charge capture (ECC).

where $\sigma_{\mathrm{EMD}}(T,F)$ represents the EMD contribution to the cross section. For this analysis, the hydrogen partial cross sections are used to define γ^F with $\gamma_{T=H}=1$. Hydrogen cross sections are used since the weak electric field of hydrogen should result in minimal EMD. The partial cross sections for the remaining targets are divided by the H partial cross sections to give γ_T for each partial cross section. The results of this division are shown in Fig. 12 for three of the targets. The results are consistent with factorization, since the values for γ_T for ΔZ from -3 to -20 are essentially constant for each target. The factorability of γ_T at larger charge changes is not as clear because of larger uncertainties and of possible contributions to the cross sections from fission, multifragmentation, and other processes, although fission is known to play a negligible role at this energy [22]. For $\Delta Z=-1$ and -2 it is apparent that there is an increase of γ_T, which becomes more pronounced for the heavier targets. This increase is consistent with an EMD contribution to one- and two-proton removal. Note that there is a significant correlation in the values of γ_T for different targets due to the common division by the H partial cross sections.

To quantify the EMD contribution, the cross sections from $\Delta Z=-3$ to -20 are fit with a single value of γ_T for each target. The values found and the reduced χ^2 of the fits are listed in Table I. Later in this section, these values will be fit with an expression, Eq. (15), incorporating a semiempirical representation of the nuclear component of the total cross sections. Using the values of γ_T and the H partial cross sections, estimates for the nuclear contributions to the $\Delta Z=-1$ and -2 cross sections are calculated for each target and subtracted from the measured cross sections. The resulting EMD cross sections are listed in Table IV. Hirzebruch *et al.* [6] found similar values using a comparable analysis. Figure 13 shows

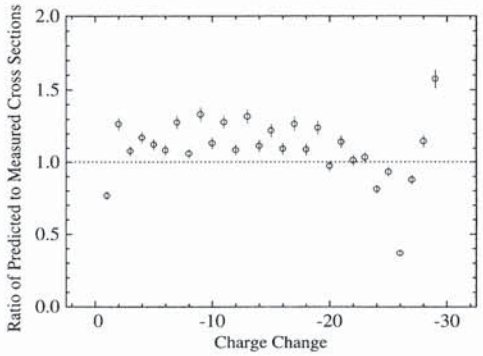

FIG. 10. Ratios of Silberberg and Tsao [8] predicted cross sections to measured partial cross sections for 10.6 GeV/nucleon Au in H as a function of charge change.

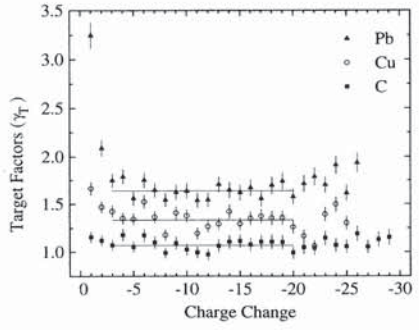

FIG. 12. Target factors for 10.6 GeV/nucleon Au on selected targets. For each target a constant target factor is fit to the $\Delta Z=-3$ to -20 target factors, shown by the solid lines. Target factors for $\Delta Z=-1$ and -2 show significant deviations from this fit, most likely due to EMD.

TABLE IV. Electromagnetic dissociation cross sections of 10.6 GeV/nucleon Au in several targets. Cross sections are derived by assuming factorization of the nuclear component of the partial cross sections as described in the text.

Target	$\Delta Z = -1$ (mb)	$\Delta Z = -2$ (mb)
C	15 ± 10	5 ± 5
Al	27 ± 9	11 ± 5
Cu	55 ± 10	13 ± 6
Sn	116 ± 12	23 ± 7
Pb	268 ± 15	42 ± 7

a plot of the sum of the $\Delta Z = -1$ and -2 EMD cross sections for each target along with the Hirzebruch *et al.* values. For these Au projectiles, these values are fit with the formula

$$\sigma_{\mathrm{EMD}}(T) = \alpha \cdot Z_T^{\beta} + \delta, \tag{14}$$

where α, β, and δ are allowed to vary. The constant term δ is used to estimate any systematic uncertainty present in the H partial cross sections. The χ^2 statistic used in the fit [23] includes the covariances among the values of γ_T, but does not include the residual covariances due to the corrections applied to the partial cross sections. The values found in the fit are $\alpha = 0.131 \pm 0.008$ mb, $\beta = 1.75 \pm 0.01$, and $\delta = 23 \pm 14$ mb with a reduced χ^2 of 0.9. The expected value of the exponent β can be calculated using the Weizsäcker-Williams method to range from ~ 1.7 to 2.0 by assuming proton photodissociation cross sections whose main strengths lie at energies varying from the Coulomb barrier to the virtual photon spectrum cutoff energy [10] of ~ 175 MeV. The low value found for β corresponds to a proton photodissociation cross section whose main strength lies near the cutoff energy. Hirzebruch *et al.* [6] found a similarly low value for β.

The sum of the EMD cross sections for each target can be subtracted from the total cross sections to give an estimate of the nuclear portion of the total cross section. Note that the EMD contributions to the total cross sections are relatively small even for the highly charged

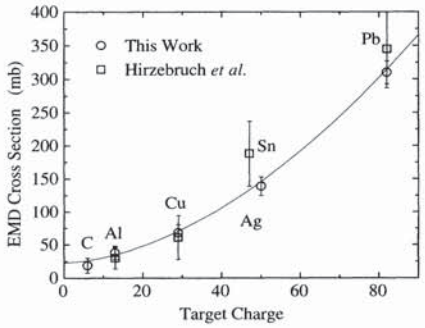

FIG. 13. Total calculated EMD charge-changing cross sections for 10.6 GeV/nucleon Au for several targets. Values from Hirzebruch *et al.* [6] are also displayed. The fitted line is Eq. (14) in the text.

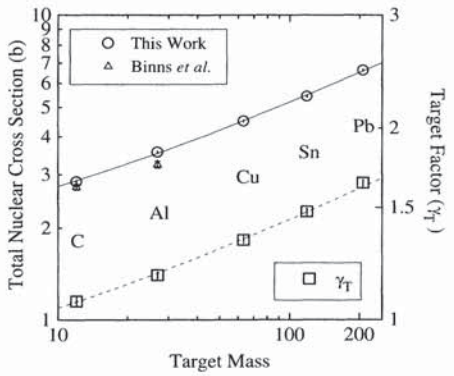

FIG. 14. The left axis is a plot of the nuclear component of the total cross section for 10.6 GeV/nucleon Au vs target mass. The solid line is a fit using Eq. (11), as explained in the text. Also displayed are the total cross sections of Binns *et al.* [3] measured at ~ 1 GeV/nucleon. The right axis is a plot of the target factors for 10.6 GeV/nucleon Au. The dashed line is a model using Eq. (15), also explained in the text.

targets (5% or less). The resulting nuclear component of the total cross sections are plotted in Fig. 14. Also shown are total cross sections measured by Binns *et al.* [3] at ~ 1 GeV/nucleon. Clearly, even if the low-energy cross sections contain EMD, they are still lower than the nuclear component of the high-energy cross sections. Thus the energy differences cannot be explained exclusively by EMD. These cross sections can be modeled by the semiempirical expressions discussed in Sec. IV A. Equation (10), with a constant overlap term, yields a fit of $r_0 = 1.362 \pm 0.006$ fm and $b = 1.05 \pm 0.04$ with a reduced χ^2 of 6.9. The covariances due to the common targetless exposure used in the calculation of the cross sections were accounted for in the χ^2 statistic [23]. For the H cross section, this expression is forced to fit by setting A_{H}, the atomic mass of H, equal to 0.079. Although the value of r_0 is comparable with the $r_0 = 1.35 \pm 0.02$ fm found in Westfall *et al.* [15], the value of b is considerably different from the $b = 0.83 \pm 0.12$ found previously, and would presumably not be a good fit to the data of Westfall *et al.*

Fitting the Binns *et al.* expression of Eq. (11) to the data gives values of $r_0 = 1.576 \pm 0.007$ fm and $d = 0.344 \pm 0.005$ with a reduced χ^2 of 3.2 and $A_{\mathrm{H}} = 0.31$, which are inconsistent with the values used previously [3,15], but give a better fit. The fit is plotted in Fig. 14. Once again, the covariance due to the common target exposure is accounted for, resulting in a higher χ^2 than simply fitting to the stated uncertainties, which are highly correlated. The fitting algorithm is unable to find a fit with a reduced χ^2 below 23 if r_0 is set to 1.35 fm.

The results of the above fits along with their previous values are listed in Table V. Although the modified Binns *et al.* expression is the best fit to the data, these fits to the present cross sections are inconsistent with those found in Binns *et al.* and Westfall *et al.* However, a value of $r_0 \sim 1.35$ fm is common to both studies and to the application of Eq. (10) to the present cross sections. This consistency, along with the good fit using the non-

TABLE V. Parameter values of Eqs. (10) and (11) from their original references and fro the fits to the total nuclear cross sections of this work. Reduced χ^2's are also listed.

	Data used in fit	r_0 (fm)	overlap	A_H	χ^2/ν
Eq. (10)	[3]	1.35	$d = 0.209 \pm 0.002$	0.089	0.42
	This work	1.576 ± 0.007	$d = 0.344 \pm 0.005$	0.31	3.2
Eq. (11)	[15]	1.35 ± 0.02	$b = 0.83 \pm 0.12$	0.089	2.9
	This work	1.362 ± 0.006	$b = 1.05 \pm 0.04$	0.079	6.9

constant overlap term of Eq. (11), implies that it may be possible to model the total charge-changing cross section by examining the energy, A_T, and A_P dependence of the hard-sphere parameters, particularly the overlap term. Attempts to fit parametrizations to a large number of total charge-changing cross sections, including the ones presented in this paper, can be found in the work of Nilsen and are also being prepared for publication [4].

Finally, the target factors γ_T, which were used to factor the partial cross sections, can be modeled with an expression incorporating a semiempirical fit to the nuclear component of the total cross sections. This type of model has been discussed in other studies [7,24]. Using the expression for $\sigma(T)$ given by the fit of Eq. (11) to the nuclear part of the total cross sections described above, the target factor is given by

$$\gamma_T = \sqrt{\sigma(T)/\sigma_0}, \tag{15}$$

where σ_0 is a normalization factor. The fit is graphed in Fig. 14 and yields a value of $\sigma_0 = 2524 \pm 93$ mb with a reduced χ^2 of 1.1. Again, covariances are taken into account.

V. CONCLUSIONS

A comparison of the charge-changing interactions of 10.6 GeV/nucleon Au with those obtained at lower energies reveal a variety of energy-dependent effects. The total charge-changing cross sections are significantly higher than those measured at lower energies, particularly for the heaviest target measured at lower energies, Al. After subtraction of EMD contributions, the total charge-changing cross sections were fit with several semiempirical expressions. The best fit resulted from an expression developed to model lower energy data, but with modified parameters.

The partial cross sections for $|\Delta Z| \leq 20$ are found to be factorable for all targets with the exception of the cross sections for $\Delta Z = -1$ and -2. The difference is explained by the occurrence of one- and two-proton electromagnetic dissociation. By assuming factorization of the nuclear part of the partial cross sections, it was possible to calculate the electromagnetic contribution to these cross sections.

The partial charge-changing cross sections differ significantly from those measured at lower energies: they are larger or equal for large charge changes and smaller for small charge changes. The H partial cross sections show an additional change from a roughly exponential form with ΔZ to a power-law relationship. These changes in the partial cross sections are large enough to seriously affect calculations of the effects of interstellar propagation on the abundances of the heaviest observed nuclei in the cosmic radiation [25]. These high-energy H partial cross sections are in closer agreement with the predictions of semiempirical calculations of Silberberg and Tsao than those at lower energies, but still differ by a significant amount.

ACKNOWLEDGMENTS

We thank E. C. Stone and B. W. Gauld of Caltech and Dana Beavis and the staff of Brookhaven National Laboratory. We also thank W. Heinrich for communication of results prior to publication. This work was supported in part by NASA and DOE.

[1] J. R. Cummings, W. R. Binns, T. L. Garrard, M. H. Israel, J. Klarmann, E. C. Stone, and C. J. Waddington, Phys. Rev. C **42**, 2508 (1990).

[2] J. R. Cummings, W. R. Binns, T. L. Garrard, M. H. Israel, J. Klarmann, E. C. Stone, and C. J. Waddington, Phys. Rev. C **42**, 2530 (1990).

[3] W. R. Binns, T. L. Garrard, M. H. Israel, M. P. Kertzmann, J. Klarmann, E. C. Stone, and C. J. Waddington, Phys. Rev. C **36**, 1870 (1987).

[4] B. S. Nilsen, Ph.D. thesis, University of Minnesota, 1994; submitted to Phys. Rev. C.

[5] C. J. Waddington, W. R. Binns, J. R. Cummings, T. L. Garrard, B. W. Gauld, L. Y. Geer, J. Klarmann, and B. S. Nilsen, Nucl. Phys. **A566**, 427c (1994).

[6] S. E. Hirzebruch, E. Becker, H. Hüntrup, T. Streibel, E. Winkel, and W. Heinrich, Phys. Rev. C **51**, 2085 (1995).

[7] Y. D. He and P. B. Price, Z. Phys. A **348**, 105 (1994); Y. He, Ph.D. thesis, University of California at Berkeley, 1993.

[8] R. Silberberg and C. H. Tsao, Appl. J. Suppl. **25**, 315 (1973); **25**, 335 (1973); R. Silberberg, C. H. Tsao, and J. R. Letaw, in *Genesis and Propagation of Cosmic Rays*,

edited by M. M. Shapiro and J. P. Wefel (Reidel, Dordrecht, 1983), p. 357.
[9] W. G. Lynch, Annu. Rev. Nucl. Part. Sci. **37**, 493 (1987).
[10] C. A. Bertulani and G. Baur, Nucl. Phys. **A458**, 725 (1986); J. D. Jackson, *Classical Electrodynamics* (Wiley, New York, 1975), p. 719.
[11] H. C. Bradt and B. Peters, Phys. Rev. **77**, 54 (1950).
[12] L. Y. Geer, Ph.D. thesis, Washington University, 1995.
[13] M. L. Cherry *et al.*, Z. Phys. C **62**, 25 (1994).
[14] B. S. Nilsen, C. J. Waddington, W. R. Binns, J. R. Cummings, T. L. Garrard, L. Y. Geer, and J. Klarmann, Phys. Rev. C **50**, 1065 (1994).
[15] G. D. Westfall, L. W. Wilson, P. J. Lindstrom, H. J. Crawford, D. E. Greiner, and H. H. Heckman, Phys. Rev. C **28**, 1602 (1983).
[16] J. C. Hill, F. K. Wohn, D. D. Schwellenbach, and A. R. Smith, Phys. Lett. B **273**, 371 (1991).
[17] J. S. Levinger, *Nuclear Photo-Disintegration* (Oxford, University Press, New York, 1960), p. 117.
[18] B. L. Berman and S. C. Fultz, Rev. Mod. Phys. **47**, 713 (1975).
[19] H. H. Heckman, D. E. Greiner, P. J. Lindstrom, and F. S. Bieser, Phys. Rev. Lett. **28**, 926 (1972).
[20] D. L. Olsen, B. L. Berman, D. E. Greiner, H. H. Heckman, P. J. Lindstrom, G. D. Westfall, and H. J. Crawford, Phys. Rev. C **24**, 1529 (1981).
[21] S. B. Kaufman, E. P. Steinberg, B. D. Wilkins, and D. J. Henderson, Phys. Rev. C **22**, 1897 (1980).
[22] C. J. Waddington, Int. J. Mod. Phys. E **2**, 739 (1993).
[23] B. P. Roe, *Probability and Statistics in Experimental Physics* (Springer-Verlag, New York, 1992), p. 180.
[24] S. E. Hirzebruch, W. Heinrich, K. D. Tolstov, A. D. Kovalenko, and E. V. Benton, Phys. Rev. C **46**, 1487 (1992).
[25] C. J. Waddington, W. R. Binns, J. R. Cummings, T. L. Garrard, L. Y. Geer, J. Klarmann, and B. S. Nilsen, Adv. Space Res. **15**, 39 (1995).